Available online at www.sciencedirect.com

ScienceDirect

Advances in Space Research 64 (2019) 2077–2087

ADVANCES IN SPACE RESEARCH (a COSPAR publication)

www.elsevier.com/locate/asr

On the difference between real-time and research simulations with CTIPe

Isabel Fernandez-Gomez [a,*], Mariangel Fedrizzi [b,c], Mihail V. Codrescu [b], Claudia Borries [a], Martin Fillion [a], Timothy J. Fuller-Rowell [b,c]

[a] German Aerospace Center (DLR), Neustrelitz 17235, Germany
[b] NOAA Space Weather Prediction Center, Boulder, CO 80305, USA
[c] CIRES University of Colorado, Boulder, CO 80309, USA

Received 26 November 2018; received in revised form 18 February 2019; accepted 19 February 2019
Available online 26 February 2019

Abstract

Understanding the thermosphere and ionosphere conditions is crucial for spacecraft operations and many applications using radio signal transmission (e.g. in communication and navigation). In this sense, physics based modelling plays an important role, since it can adequately reproduce the complex coupling mechanisms in the magnetosphere-ionosphere-thermosphere (MIT) system. The accuracy of the physics based model results does not only depend on the appropriate implementation of the physical processes, but also on the quality of the input data (forcing). In this study, we analyze the impact of input data uncertainties on the model results. We use the Coupled Thermosphere Ionosphere Plasmasphere electrodynamics model (CTIPe), which requires satellite based solar wind, interplanetary field and hemispheric power data from ACE and TIROS/NOAA missions. To identify the impact of the forcing uncertainties, two model runs are compared against each other. The first run uses the input data that were available in real-time (operational) and the second run uses the best estimate obtained in post-processing (research or historical run). The analysis is performed in a case study on the 20th November 2003 extreme geomagnetic storm, that caused significant perturbations in the MIT system. This paper validates the thermosphere and ionosphere response to this storm over Europe comparing both CTIPe model runs with measurements of Total Electron Content (TEC) and thermosphere neutral density. In general, CTIPe results show a good agreement with measurements. However, the deviations between the model and observations are larger in the ionosphere than in the thermosphere. The comparison of the two model runs reveals that the deviations between model results and measurements are larger for the operational run than the research run. It is evident for the storm analyzed here, that data gaps in the input data are impacting considerably the model performance. The consistency between simulation and measurements allows the interpretation of the physical mechanisms behind the ionosphere perturbations and the changes in neutral composition during this event. Joule heating in the Auroral region, generating meridional winds and large scale surges, is suggested to be the main driver of the positive ionospheric storm over central Europe. In the polar cap and Auroral region, convection processes dominate the thermosphere-ionosphere conditions. This study does not only illustrate the importance of working with a good estimate of the model forcing, but also indicates the necessity of using measurements and models, to get a better understanding of the most likely responsible processes for the observed storm effects.
© 2019 COSPAR. Published by Elsevier Ltd. This is an open access article under the CC BY license (http://creativecommons.org/licenses/by/4.0/).

Keywords: CTIPe model; Operation vs. research simulations; Model forcing; 20th November 2003; Storm dynamics

* Corresponding author.
E-mail addresses: Isabel.FernandezGomez@dlr.de (I. Fernandez-Gomez), mariangel.fedrizzi@noaa.gov (M. Fedrizzi), mihail.codrescu@noaa.gov (M.V. Codrescu), Claudia.Borries@dlr.de (C. Borries), tim.fuller-rowell@noaa.gov (T.J. Fuller-Rowell).

https://doi.org/10.1016/j.asr.2019.02.028
0273-1177/© 2019 COSPAR. Published by Elsevier Ltd.
This is an open access article under the CC BY license (http://creativecommons.org/licenses/by/4.0/).

1. Introduction

The ionosphere is embedded in the Earth's upper atmosphere in the altitude region between 60 and 1000 km. It is characterized by the permanent presence of free electrons, as the result of low atmospheric density and ionizing effects of solar and cosmic radiation and particle precipitation. The physical processes in the ionosphere are strongly related to conditions in the magnetosphere and thermosphere. We therefore speak of a coupled magnetosphere-i onosphere-thermosphere (MIT) system.

Solar activity, i.e. coronal holes, coronal mass ejections (CME), strong flares and energetic proton events can generate disturbances in the MIT system. In the ionosphere, this is identified with changes in the electron density structure, that can either be enhancements (positive ionospheric storm) or depletion (negative ionospheric storm) of the F2-layer electron density and the Total Electron Content (TEC) compared to quiet conditions. These perturbations have a significant impact on communication and positioning systems, disrupting or even rendering them unusable. To avoid its impact on the performance and reliability of space-borne and ground-based communication and navigation systems, it is necessary to understand and be able to predict the behavior of the MIT system.

The most fundamental mechanisms contributing to the generation of the ionospheric response to storm disturbances are properly known: changes in convective electric fields imposed by the magnetosphere at high-latitudes, changes in neutral composition (Prölss and von Zahn, 1977), changes in neutral winds and temperature (Fuller-Rowell et al., 2018), prompt penetration and dynamo electric fields (Blanc and Richmond, 1980; Balan et al., 2009; Mannucci et al., 2008; Shimeis et al., 2015) and high latitude particle precipitation (Fuller-Rowell et al., 1994; Prolss and Bird, 2004). Studies and models of how the MIT system reacts to storm conditions are of great interest and there have been numerous publications on this topic (Codrescu et al., 1992; Buonsanto, 1999; Mansilla, 2004; Blanch et al., 2005; Jakowski et al., 2012). However, the contribution of the individual mechanisms depends strongly on the properties of solar energy input and on the prevailing thermosphere conditions.

Physics based models are capable to estimate the thermosphere-ionosphere conditions based on solar wind, interplanetary magnetic field (IMF) and solar irradiance proxies. One example is the Coupled Thermosphere - Ionosphere - Plasmasphere model with self-consistent electrodynamics (CTIPe) (Fuller-Rowell et al., 1996; Millward et al., 1996, 2001). The provision of reliable measurements of the external drivers (solar wind, IMF, etc.), which are used as forcing for the model, is expected to be of great importance. However, CTIPe runs in real-time and real-time input data does not always have the best quality. To study the impact of decreased quality of the input data, we investigate the difference in model results based on operational (real-time) input data and the best estimate (research) input data, which is provided after reprocessing and quality check. We are going to discuss how well the model deals with uncertainties in the solar wind energy inputs, their spatial distribution and the large number of interacting processes. In a representative case study, we analyze CTIPe simulations for one of the most intense storms of the recent decades, the 20th November 2003 storm. CTIPe results are compared against observations of thermosphere and ionosphere, i.e. neutral density from accelerometer measurements for the thermosphere and TEC derived from GNSS measurements for the ionosphere, which are standard parameters for model validation.

The performance of CTIPe is documented in e.g. Codrescu et al. (2008) and Negrea et al. (2012). However, until a few years ago, the reproduction of extreme storms have been a considerable challenge for CTIPe and thus the performance of CTIPe was weaker compared with other physics based models (Shim et al., 2012). But recently, CTIPe code has been improved with modifications in the small scale variability in convection electric fields, the NO cooling and the lower boundary conditions. Now, CTIPe results compare well with the performance of other physics based models (Shim et al., 2018). With the comparison of model results and measurements for the extreme storm on the 20th November 2003, we aim to further extend the demonstration of the new CTIPe capabilities and improved performance.

The 20th November 2003 geomagnetic storm had remarkable effects on the Earth's ionosphere. Baishev et al. (2008) reported strong energy deposition leading to enhanced ionospheric auroral currents. Ebihara et al. (2005) describe the magnetosphere-ionosphere coupling during this storm, suggesting that enhanced convection electric fields generate a very intense ring current. In good agreement, Foster et al. (2005) report strong cross polar cap convection and the presence of the tongue of ionization (TOI) in that area, transporting plasma from the dayside to the nightside ionosphere. De Franceschi et al. (2008) revealed strong enhancements and steep gradients in TEC during nighttime under a prevailing negative B_z component of the interplanetary magnetic field (IMF). A positive storm observed in TEC and foF2 in the European-African sector at 12 UT has been reported e.g. in Crowley et al. (2006) and Borries et al. (2017). Strong dynamics (generation of wind surges, steep gradients and significant increase of the equivalent slab thickness) related to heating processes in the Auroral region have been indicated in Borries et al. (2017). They confirmed a close vicinity of the location of the eastward Auroral electrojet, the mid-latitude trough, the source region of the surges, gradients in TEC and foF2 and precipitation. The authors also discuss the significant equatorward shift of the surges source region and explain it with the expansion of the Auroral oval related to a strong compression of the plasmasphere (Bortnik et al., 2006). The global thermosphere-ionosphere (TI) response to the onset of the 20th November 2003 geomagnetic storm has been

explored in Crowley et al. (2006) using the NCAR TIME-GCM. Their simulation of the 12 UT period using the TIME-GCM reproduced drastic thermospheric equatorward winds in the European-African sector. These were forced by high-latitude heating processes associated with the storm. The authors suggest that the neutral winds drive the ionospheric plasma to higher altitudes, where the ratio of production to loss is greater, leading to enhanced electron densities in the sunlit sector. In this study, CTIPe is going to be used to complement the discussion on the storm driving effects in the TI system. Special attention will be paid to the high latitude heating, winds and convection processes.

In summary, this study aims to investigate the application of the CTIPe model in a case study on the extreme 20th November 2003 geomagnetic storm, targeting the following three objectives: 1. Estimate the importance of the model forcings and its impact on the model results. 2. Assess the capabilities of CTIPe to reproduce correctly the thermosphere-ionosphere during extreme conditions. 3. Better understand the driving mechanisms for ionospheric storms, focusing on the European sector (10°E, 30–70°N).

2. Database and methods

2.1. CTIPe model

The global three-dimensional time - dependent CTIPe model (Fuller-Rowell et al., 1996; Millward et al., 1996, 2001) is a physics based, nonlinear, numerical code developed and maintained at the National Oceanic and Atmospheric Administration (NOAA) Space Weather Prediction Center (SWPC) to support operational nowcasting and forecasting algorithms for space weather. The code solves the momentum, energy and composition equations for the neutral and ionized atmosphere. It consists of four fully coupled components running concurrently: The thermosphere developed initially by Fuller-Rowell et al. (1996), a high-latitude ionosphere (Quegan et al., 1982), a mid and low-latitude ionosphere-plasmasphere (Bailey, 1983), and the electrodynamics developed by Richmond et al. (1992) and included by Millward et al. (2001).

Fig. 1 represents a schematic view of CTIPe components and inputs. The thermospheric code (T) solves the general circulation equations for the global thermosphere on a non-inertial geographic frame of reference rotating with the Earth. The calculations are performed on a discrete grid of 2° latitude and 18° longitude resolution and on 15 pressure levels in the vertical direction, from a lower boundary of 1 Pa assumed at about 80 to more than 400 km altitude. The high latitude ionosphere (I) (above 55° N/S) and the mid-low latitude ionosphere - plasmasphere (I-P) components have been implemented as separate modules because of their structure of open (I) and closed (I-P) field lines. They both use a semi-Lagrangian scheme but have independent time steps and different resolutions. The electrodynamics scheme is calculated on a 5° by 5° grid, every 15 min.

The magnetospheric input is based on the statistical models of auroral precipitation and electric field described by Fuller-Rowell and Evans (1987) and Weimer (2005), respectively. The auroral precipitation is keyed to the hemispheric power index (also called Precipitation index, PI (Foster et al., 1986)), based on TIROS/NOAA auroral particle measurements. The Weimer electric field model is driven by solar wind parameters affecting the Earth's magnetosphere. These drivers are specified at one minute cadence based on L1 solar wind measurements from Advanced Composition Explorer (ACE) satellite. Included are the magnitude and direction of the IMF in the y-z plane, together with the velocity and density of the solar wind. It uses the Whole Atmosphere Model (WAM) as a lower boundary condition at 80 km (1 Pa), and it also incorporates an empirical model for NO (Nitric Oxide) (Marsh et al., 2004), used to calculate NO cooling, and a small-scale electric field fluctuations component for the calculation of Joule Heating (Codrescu et al., 1995). The CTIPe ionosphere results include the major ion species H^+ and O^+ for all altitudes, and other molecular and atomic ions N_2^+, O_2^+, NO^+ and N^+ below 400 km.

CTIPe has been shown to appropriately model the upper atmosphere total mass density response to geomagnetic activity (Fedrizzi et al., 2012) and the NmF_2/hmF_2 measurements from several ionosondes around the globe. Previous studies have been used to improve its results based on the knowledge and analysis of systematic and seasonal model biases (Negrea et al., 2012).

2.2. GNSS measurements

The accuracy of Global Navigation Satellite Systems (GNSS) depends on the electron density distribution in the Earth's ionosphere, since it will change the path and velocity of radio waves. Commonly, GNSS measurements are used to determine the total number of electrons along a path between the receiver and radio transmitter (TEC) and generate TEC maps. TEC is defined as the integrated electron density along the ray path, and it is measured in electrons per square meter (1 TECU = 10^{16} electrons/m^2). In this study, GNSS based TEC data provided by the International GNSS Service (IGS) is used. It is a well accepted data source which has continuous quality monitoring.

2.3. CHAMP satellite

This study also focuses its attention on neutral mass density products derived from the measurements of the accelerometer on board of the CHAllenging Minisatellite Payload (CHAMP) mission. The processing of the accelerometer data (Bruinsma et al., 2004; Doornbos et al., 2010) involves a calibration using GPS tracking data, removal of the acceleration induced by the thrusters as well

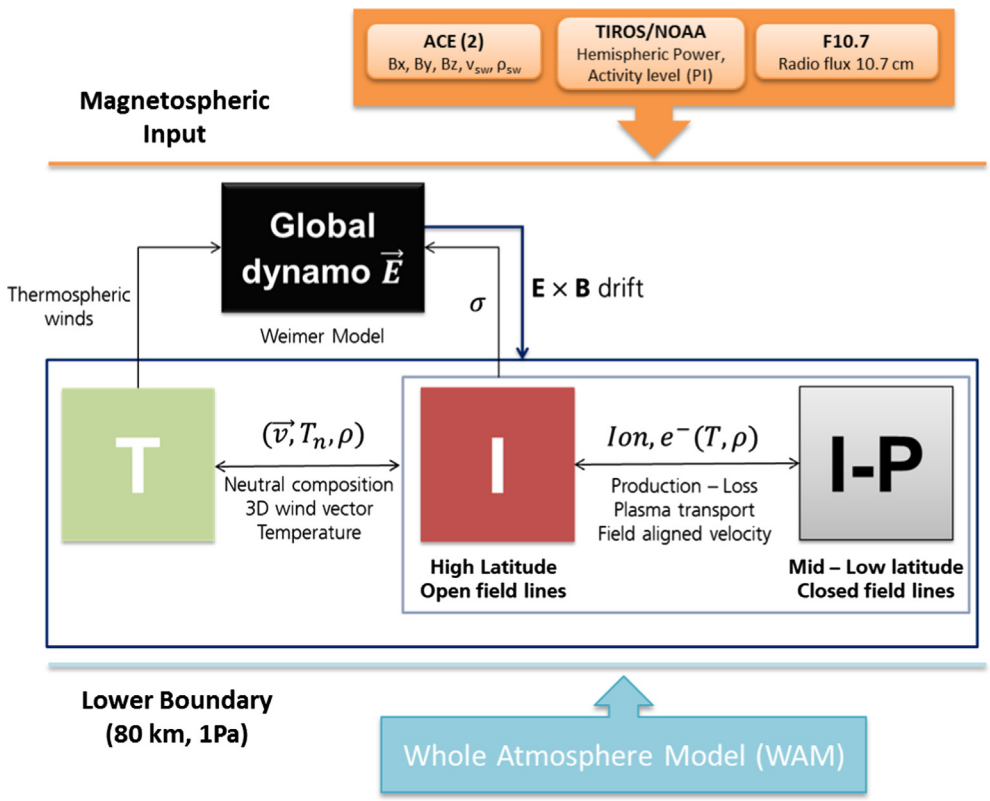

Fig. 1. Schematic view of CTIPe working flow: (T) is the thermospheric code, (I) the high-latitude ionosphere model with open field lines and (I-P) represents the mid-low latitude ionosphere-plasmasphere model with closed field lines.

as the one induced by the radiation pressure force and requires the modelling of the action of the aerodynamic force on the spacecraft. Thermospheric density data are available on the DEOS Thermosphere web server. They are provided along the orbit with a 10-s temporal resolution which corresponds approximately to 100 km. We consider the period of time from 19 to 21 November 2003. At this time, the average local time for the CHAMP satellite is 23 LT for the ascending orbit and 11 LT for the descending orbit and the average altitude of flight is about 400 km.

To find a matching CTIPe value for each CHAMP observation, we first search the closest element according to latitude. We then look for the adjacent points with respect to longitude to obtain two 2-dimensional matrices, one for each longitude, that depend on altitude and time. With these two matrices stacked together, we perform a second order spline interpolation in three dimensions to obtain a vertical neutral density profile for each time step at the CHAMP measurement longitude and latitude.

Subsequently, as CTIPe output grid height levels do not match CHAMP satellite altitude, we seek for the best estimation of the model neutral mass density prediction at the satellite height. To obtain that value, we assume atmospheric hydrostatic equilibrium and thus an exponential decrease of neutral mass density with increasing height. The assumption holds because CTIPe is a hydrostatic model which deals only with average quantities in quasi steady - state. The CHAMP satellite can fly either below or above the model's upper boundary since CTIPe constant pressure levels change in height depending on solar activity. In the first case, a linear interpolation of the logarithm of the neutral mass density is performed. However, if the satellite flies above, we extrapolate calculating the neutral mass density ρ as:

$$\rho = \rho_{upper} * \exp(-(h - h_{upper})/H) \quad (1)$$

where h is the height of the satellite, ρ_{upper} is the neutral mass density at CTIPe upper boundary h_{upper}. The height scale H is defined as $H = RT/gM$, where R the gas constant, T the average temperature, g the gravitational constant and M the mean molecular mass of the neutral atmosphere. This height scale is calculated using the temperature and the mean molecular mass at CTIPe upper boundary.

Once CTIPe prediction has been estimated for a specific latitude, longitude and height, the resulting time series is resampled to a one-minute resolution using linear interpolation. The final CTIPe prediction is taken to be the closest value with respect to the time of the CHAMP measurement.

3. Storm morphology

Two periods of enhanced solar activity occurred during October and November of 2003 that produced strong geomagnetic storms. They were primarily caused by two

massive sunspot groups that produced intense X-class flares and large CMEs (Blanch et al., 2005). The second period, corresponding to the 19–22 November 2003 contains one of the most severe geomagnetic storms ever recorded.

The Disturbance storm time index (Dst) can be used as a proxy of the geomagnetic storm magnitude and it is a good indicator of the storm phases in time (upper panel Fig. 2). The disturbance has a rapid onset on 20.11.2003 at 8 UT, which is about the time of the sudden storm commencement (SSC). The main phase took from 8 to 23 UT (shadowed area), with a sharp decrease of Dst to a minimum below −400 nT, and a recovery phase that lasted until 24 UT of the following day (22.11.2003). Dashed lines indicate storm and superstorm conditions (−50 nT and −200 nT respectively). The Auroral Electrojet index (AE) in the middle panel, shows enhancements indicating heating processes in high latitudes. An intermediate recovery occurred between 10:45 UT and 12 UT, when Dst increase and AE decreased. However, maximum Dst value during this intermediate recovery did not reach values of quiet conditions. The 3 h Kp index (lower panel) quantifies the disturbances in the horizontal component of the Earth's magnetic field, with values larger than four indicating a geomagnetic storm.

4. Operation vs. research

4.1. Magnetospheric input

The values of the CTIPe input parameters are illustrated in Fig. 3 for both operational (red) and research (blue) runs and for the quiet and storm days. Represented from top to bottom are: the total IMF B_t, the IMF B_z component, solar wind speed and density as measured by NASA's Advanced Composition Explorer (ACE), and the activity level (PI) and total hemispheric power in GW from the TIROS/NOAA satellites. It is visible in this figure that TIROS/NOAA data does not differ between operational and research. But there is a significant difference for ACE data. Energetic particles can introduce noise in the ACE detector and make the signal fluctuate. The solar wind density is particularly sensible to this effect. Because of these, no ACE data is available in real-time, and the code repeats the last reliable 10 min until the satellite is operative again. The NOAA Space Environment Services Center establishes a Solar Proton Event (SEP) occurring the 20th November 2003 that can explain the missing data of the ACE parameters during the main phase of the storm. However, the data gap for the quiet day cannot be explained with this effect. In this case the missing data could be due to communication or computer problems occurring in real-time. The values for the research input are corrected with the OMNI data in post processing, introducing clear disparity between operational and research magnetospheric inputs. During the second day, storm characteristics can be observed in all the parameters (shadowed area) Increasing B_t, B_z

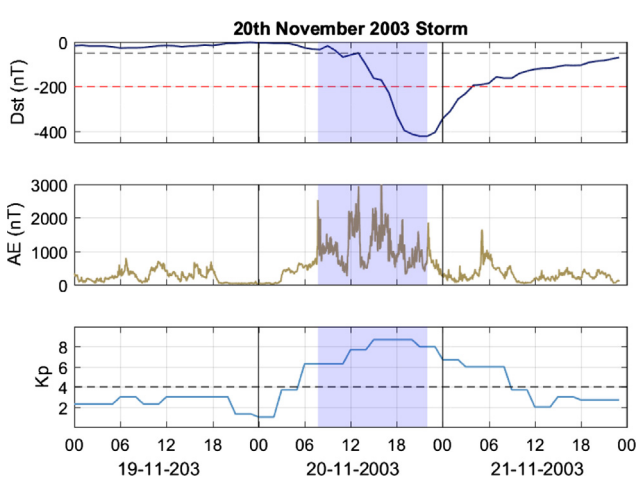

Fig. 2. Dst index (upper panel) for the days of the storm 19–21 November 2003. The large drop to −472 nT shows characteristics of a superstorm event ($D_{st} < -200$ nT red line) during the second day (20.11.2003). The Dst main phase of the storm is represented by the shadowed area. The Auroral electrojet (middle panel) displays a sudden increase after the storm onset. Kp index (lower panel) shows disturbed conditions $Kp > 4$ at 6 UT. (For interpretation of the references to color in this figure legend, the reader is referred to the web version of this article.)

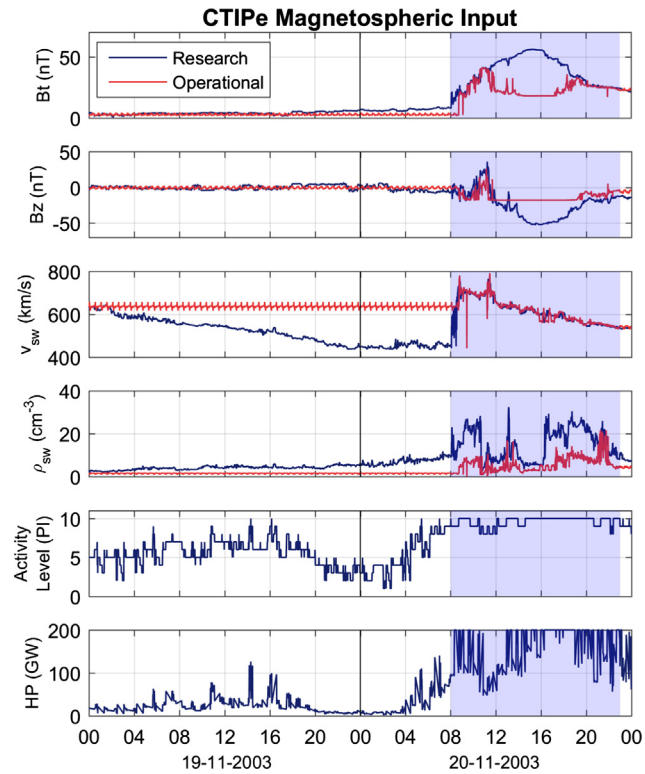

Fig. 3. CTIPe operation (red) and research (blue) magnetospheric inputs for the 19–20 Nov 2003 storm: total IMF B_t, IMF B_z, solar wind speed and density, measured by ACE satellite and the activity level (PI) and total hemispheric particle precipitation power (GW) from TIROS/NOAA. The shadowed area represents storm main phase, according to D_{st} index. Considerable differences are found for real-time and research ACE parameters. (For interpretation of the references to color in this figure legend, the reader is referred to the web version of this article.)

component negative values, sudden rise of the solar wind velocity and density, as well as an increase in the hemispheric power and activity level. These storm traits are detected for both inputs, however, discrepancies between operational and research B_t, B_z and solar wind density can be observed at storm time. The impact of these operational - research discrepancies in the magnetospheric conditions during storm time on the model results are investigated in this study.

4.2. Observations in the thermosphere: neutral mass density

To evaluate the changes in the thermosphere during storm conditions, we use CHAMP neutral mass density measurements along the satellite orbit. Fig. 4 presents the comparison of the orbit average neutral mass density ρ derived from CHAMP accelerometer data (black) with the ρ results of CTIPe. Operational (red) and research (blue) runs are represented. The very significant increase of ρ, generated by the storm disturbances, starts at about 12 UT on 20th November, reaching a maximum five times bigger than quiet values. In general, both model runs simulate very well the neutral density change binned to storm main phase with not more than 8.4 % deviation from the CHAMP measurements. Nevertheless, some discrepancies between the operational and research run are visible during the maximum peak of the storm. The research run goes closer to CHAMP measurements during the storm disturbance with a peak difference of 0.07, an average difference of 0.02 and an RMSE of 0.06×10^{-11} kg m^{-3} (Table 1). Then, we can assume that ρ is reproduced better by CTIPe research run, fitting during quiet time and storm main phase. Thus, considering the good agreement of the CTIPe results with the thermospheric density measurements, a good representation of thermosphere conditions can be assumed.

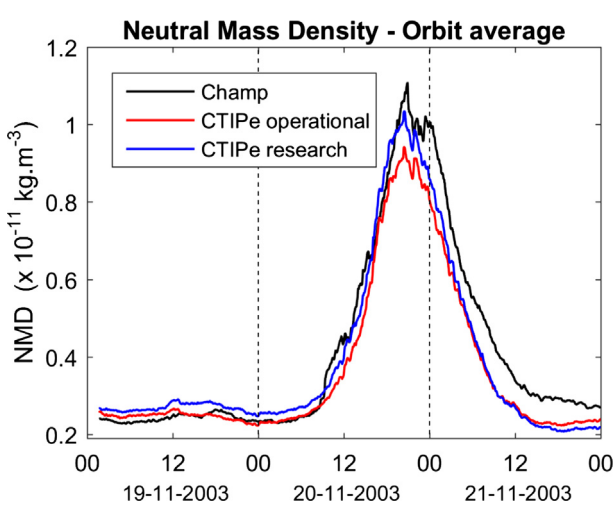

Fig. 4. Comparison of orbit average neutral mass density CHAMP (black) and CTIPe operational (red) and research (blue) for the 19 to the 21st of November 2003 storm. (For interpretation of the references to color in this figure legend, the reader is referred to the web version of this article.)

4.3. Observations in the ionosphere: TEC

Fig. 5 depicts the change in latitude vs. time of the TEC for a fixed longitude centered over Europe (10° East). The top and middle rows represent the TEC obtained from the CTIPe model operational and research run respectively. The lower row corresponds to the TEC retrieved from GNSS ground-based receiver data. The columns illustrate, the quiet and storm days 19–20.11.2003 and the difference between storm time and quiet time.

In the figure, we can identify first, the positive phase of the storm following the storm onset (dashed line). The enhancement starts at high latitudes and travels equatorward with time during the main phase of the storm. At 30° N, the positive storm starts at about 10 UT, and it is well visible in the model runs and measurements. The TEC increases dramatically by 20 TECU at 13:30 UT and 40°N for IGS observations and CTIPe research run, however the variation for the operational run is 12 TECU less. Then, while the operational run underestimates the positive storm, the research run underestimates TEC at mid-latitudes and overestimates it at low latitudes. Second, it can be observed a depletion area initially located at high latitudes at 70°N at 12 UT that dislocates equatorward to lower latitudes (40°N 18 UT for IGS and a 20 UT for CTIPe) during storm day. This area has been proven to coincide with the trough region (Borries et al., 2017). Third, during the evening there is a TEC enhancement occurring at high latitudes (northward of the trough) that is best visible at the difference between the storm and quiet day IGS TEC (right panels). This enhancement is also replicated by CTIPe but with significant lower amplitude.

A better estimation of the discrepancies between model and observations is obtained analyzing the TEC time series for one fixed location. At Fig. 6, IGS TEC is represented in black, CTIPe operational run in red and research simulation in blue for 10°E and 40°N. Significant differences between operational and research run can be identified. The operational maximum peak divergence is almost 28 TECU, the average differences is 7.5 and the RMSE is 10.8. In comparison, the research simulation shows better results (Table 2) with a 17% deviation from measurements.

5. Discussion of CTIPe capabilities

CTIPe has proven to reproduce very well the thermosphere density (c.f. Fig. 4). The only difference, which was detected, is that CTIPe recovers a little bit earlier than CHAMP. This early recovery can be attributed to a slight overestimation of the NO cooling. However, the NO cooling in CTIPe must to be fairly good to achieve this good agreement with CHAMP measurements.

Regarding the ionosphere, the results display certain differences between the TEC estimations of the model and the measurements. In Fig. 5, one can notice a transition area in about 55°N, which is about the region of the transition between the CTIPe I-P and I-components. This transition

Table 1
CHAMP and CTIPe neutral mass density statistics for operational and research runs. Shown are the peak difference, the average difference, and the root mean square error (RMSE).

	Operational ($\times 10^{-11}$ kg m^{-3})	Research ($\times 10^{-11}$ kg m^{-3})
Peak Diff	0.17	0.07
Average Diff	0.05	0.02
RMSE	0.08	0.06

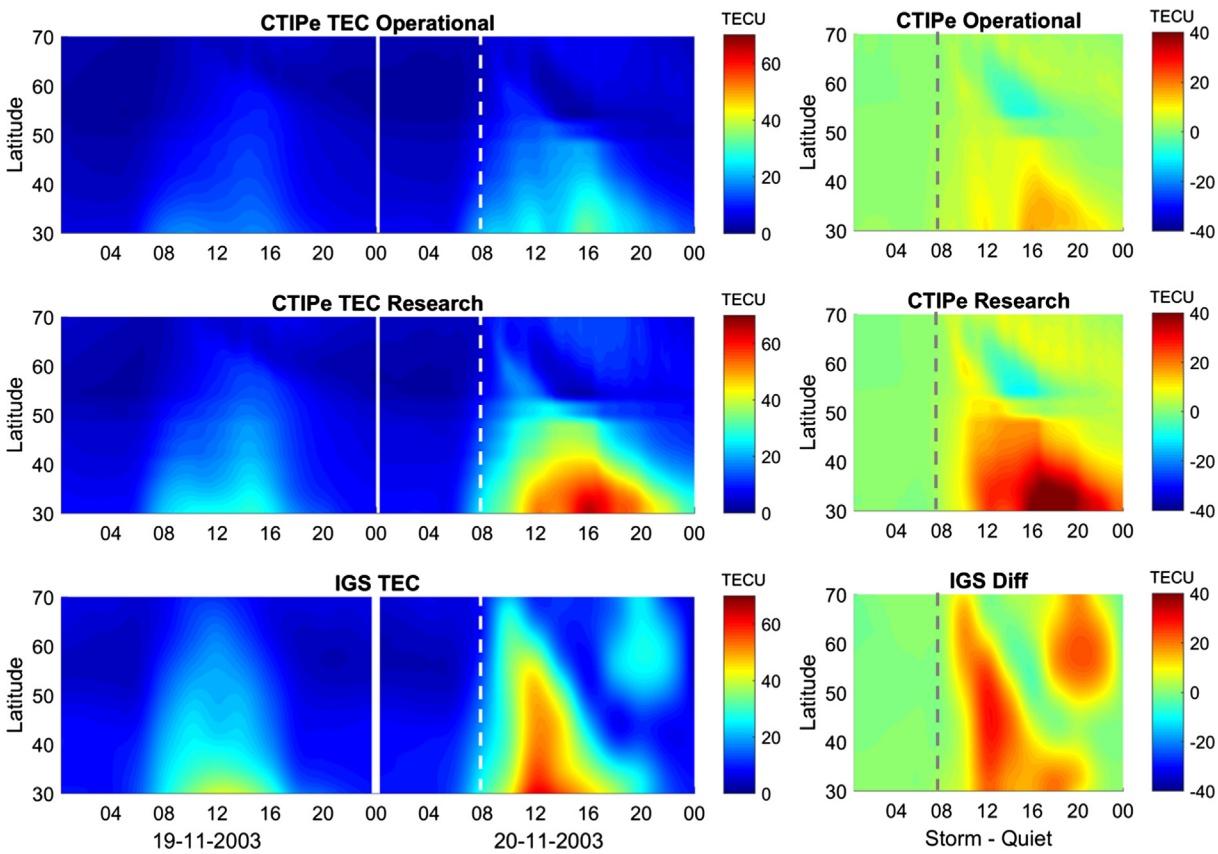

Fig. 5. TEC latitude vs. time calculated with CTIPe model (upper and middle rows) and IGS TEC maps (lower row), over the European sector (10°E longitude) for the quiet and storm day (19–20.11.2003). Differences of over 20 TECU from quiet to storm time can be seen from IGS measurements and CTIPe research run.

region causes artificial TEC changes between the high latitude ionosphere and the mid-low latitude ionosphere at 55° N. This indicates a different impact of plasmasphere and ionosphere model components, which is especially visible during extreme storm conditions. In high latitudes (I model component) the amplitude of the trough is reproduced well. When the Auroral oval extends and the trough relocates to mid-latitudes (I-P model-component), the amplitude is not reproduced well anymore. Missing plasma transport between both model components is expected to cause the artificial TEC gradients around 50° N and the wrong representation of the trough amplitude in the model results. The implementation of improved transport processes between the I and I-P model components in the transition region (30–50° N) should help to improve the model results during storm conditions.

For a good representation of electron densities, the correct estimation of electric fields is of great importance. This version of the CTIPe code does not implement Prompt Penetration Electric Fields (PPEF). This can be an additional cause of the underestimation of TEC in the results shown in Figs. 5 and 6. The enhancement of CTIPe with PPEF computation is expected to improve the model results during storm conditions.

At high latitudes during night (18–24 UT), CTIPe exhibits lower TEC compared to the IGS TEC maps. This region is considered to be within the Auroral oval, where strong plasma convection processes dominate. The reduced TEC in this region might be an indication that CTIPe does not represent the momentum transfer from ion drag well enough yet.

6. Dynamics in the thermosphere - ionosphere system

We have seen that TEC increased significantly as a response to the onset of the November 2003 storm

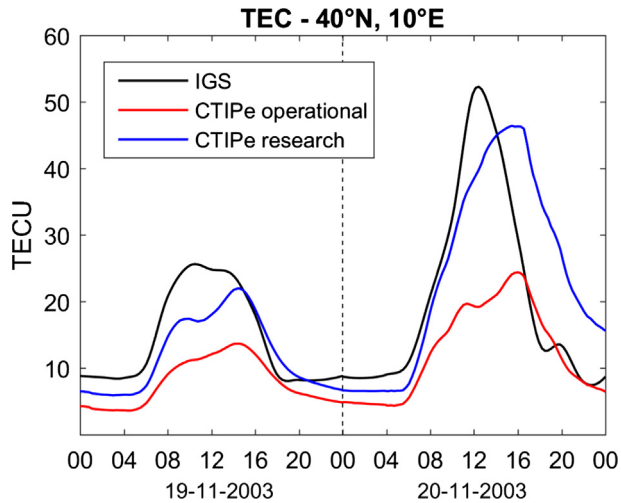

Fig. 6. TEC time series for 10° longitude and 40° latitude, for quiet and storm day (19–20.11.2003). Represented are IGS observations (black), model operational (red) and research (blue) results. (For interpretation of the references to color in this figure legend, the reader is referred to the web version of this article.)

Table 2
GPS and CTIPe TEC statistics for operational and research runs. Show are the peak difference, the average difference, and the root mean square error (RMSE).

	Operation (TECU)	Research (TECU)
Peak Diff	27.9	7.5
Average Diff	5.9	0.4
RMSE	10.8	7.2

(Fig. 5). A set of CTIPe thermospheric parameters are presented in Fig. 7 to discuss the related perturbations. These parameters correspond to the CTIPe research run, as we have seen that proper estimates of the magnetospheric input produce results closer to the observations.

CTIPe reproduces strong perturbations in Joule heating over Europe. They can be observed in the latitude vs. time plot of Joule heating at F_2 layer altitude for the quiet and storm day 19–20.11.2003. During the geomagnetic storm, the IMF B_z descend to negative values (Fig. 3), increasing the cross polar cap potential drop and as a consequence, intensifying the magnetospheric electric fields. In addition, the impact of high energy particles into the auroral zone leads to a boost of the energy flux (Foster et al., 1986). Both effects combined, drive to electric currents and strong Joule heating of the atmospheric gases. More than 75% of the energy deposited from the magnetosphere into the TI system during storms comes from Joule heating (Rodger et al., 2001) while the rest is from momentum transfer from ion drag. This makes Joule heating the most significant energy deposition mechanisms during storms.

The obvious response to this energy input is a rapid increase in temperature. The traces due to the Joule heating can be seen in the temperature perturbation. However, the temperature is also under the influence of transport by the wind field and losses by heat conduction and radiation. In

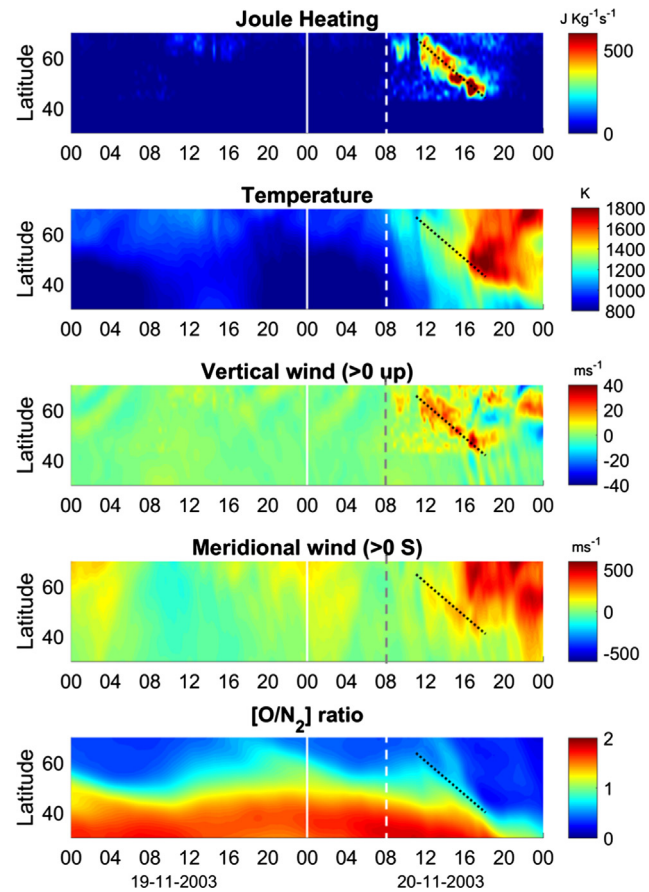

Fig. 7. Latitude vs. time of the storm 19–20.11.2003 over Europe (10°E), at the F2 region (~ 272 km) for Joule heating, neutral temperature, vertical wind, meridional wind and integrated atomic Oxygen to molecular Nitrogen ratio. The storm onset is represented by a dashed line and Joule heating path by a black line.

this way the temperature distribution will be not an exact image of the Joule heating (Fuller-Rowell et al., 1994). This increase in temperature causes expansion of the atmosphere, upwelling of the neutral atmosphere above the heating region (vertical winds), and the launch of surges with effects in both the thermosphere and ionosphere. The signatures of these atmospheric surges are visible in the winds (Fig. 7), moving equatorward with speed $616 \pm 10\ \mathrm{ms}^{-1}$, in good agreement with the speed of traveling ionospheric disturbances $629 \pm 49\ \mathrm{ms}^{-1}$ reported by Borries et al. (2017). Behind the surge, a large scale storm circulation is added to the quiet time global circulation and these enhanced winds contribute to global ionospheric storm effects as reported in Crowley et al. (2006). This storm wind cell reverses the meridional winds at noon, (they have been negative on the 19_{th} and positive - equatorward on the 20_{th}), starting at the equatorward edge of the Joule heating region.

At high latitudes beginning after 15 UT, northward to the Joule heating region, CTIPe reconstructs strong temperature enhancements (increasing more than 1000 K) and equatorward winds (up to $500\ \mathrm{ms}^{-1}$). This indicates ion driven winds across the polar cap. The results of

Foster et al. (2005), who clearly point out a TOI and cross polar convection, support this suggestion. However, since IGS TEC is significantly larger than CTIPe (Fig. 5), the model still seems to underestimate this effect.

The rapid heating of the neutral atmosphere causes expansion, upwelling, and the departure from diffusive equilibrium of the neutral atmosphere, increasing the mean molecular mass, and as a consequence, a decrease in the ratio of integrated Oxygen to molecular Nitrogen $\sum[O/N_2]$ densities (Buonsanto, 1999). $\sum[O/N_2]$ changes are one of the main parameters to interpret the neutral atmosphere composition disturbances during a geomagnetic storm and its global behavior for this storm has been studied in depth by Crowley et al. (2006), Meier et al. (2005), Kil et al. (2011). The well known seasonal asymmetry (Qian et al., 2009), caused by a characteristic wind pattern, determines that the largest band of $[O/N_2]$ will be in the winter hemisphere (North) during quiet days. This band moves equatorward in the course of the main phase of the storm (20.11.2003), driven by the enhanced storm circulation. The decreased values of the polar region, the neutral composition bulge, also travels towards the equator in the second half of the day. Similar $\sum[O/N_2]$ conduct has been observed by Global Ultraviolet Imager (GUVI) satellite during this storm (Crowley et al., 2006). The redistribution of the composition causes the increase of neutral mass density with a maximum up to 1.2×10^{-11} kg m^{-3} (Fig. 4).

The ionosphere response to the storm effects is rather complex. Between 8 and 16 UT, an intense positive ionospheric storm was present in central Europe (mid latitudes, Fig. 5 inner panel). During this time, enhanced equatorward winds were present (Fig. 7) pushing the plasma up along the magnetic field lines to regions with decreased recombination. Additionally, the winds transport oxygen rich air to mid-latitudes causing an increase of $[O/N_2]$. A corresponding slight rise can be observed in Fig. 7. The increased $[O/N_2]$ ratio contributes to the positive ionosphere storm in mid-latitudes. High latitudes are characterized by a considerable reduction of $[O/N_2]$ ratio after 16 UT. Usually, a decrease in $[O/N_2]$ results in a decrease in electron density. But the contrary takes place in the high latitude evening ionosphere (20th Nov 16–24 UT, 50–70°N), where Fig. 5 shows an increase of TEC. Strong plasma transport across the polar cap, driven by a convection electric field, causes the increase of TEC. This strong plasma transport is reflected in the ion driven winds (severe equatorward winds in high latitudes discussed before) and the strong heating in the same region caused by collision and friction.

7. Summary and conclusions

In this study we addressed three questions, the importance of the model forcings accuracy, the model capabilities and storm driving mechanisms using CTIPe model in comparison with neutral density data derived from CHAMP and TEC data provided by IGS. We analyzed it for the extreme storm on the 20th November 2003 case study.

The impact of model forcing has been studied by comparing model results generated with different magnetospheric input data. The results show that the discrepancies between model and measurements increase with the increase in the uncertainties of the magnetospheric input data as demonstrated with the CTIPe operational and research runs. The impact on the ionosphere TEC is significantly larger than the impact on the thermosphere density. This indicates the importance of the correct estimation of the model forcing. Especially for the generation of operational model results, the provision of reliable solar wind and IMF data is crucial. Because current instruments are not robust enough to provide continuous data, they are a limiting factor for operational model results at the moment. Data assimilation is a possibility to overcome this limitation and obtain a better estimate of the forcing.

The model capabilities have been assessed by examining the deviation between model results and thermosphere-ionosphere measurements. It has been shown that there is generally a good agreement between the model and measurements. The thermosphere seems to be better portrayed than the ionosphere. The neutral density is accurately reproduced by CTIPe. Only a moderately faster recovery of the thermosphere density has been indicated, which may result from a slight overestimation of NO cooling. Because of the complexity of electrodynamics processes in the ionosphere, it is a greater challenge to reproduce well the electron densities with numerical modelling. This is in fact reflected in the CTIPe outcome. In the ionosphere, the discrepancy between the model and observations is larger than in the thermosphere. Following potential sources of the underestimation of TEC have been identified: To a certain portion, this seems to result from a lack of plasma transport in the transition region between the I- and I-P model-components. Also, the absence of PPEF implementation is considered as a limiting factor for the correct TEC calculation. Finally, the TEC in the polar cap and Auroral region is underestimated by the model. Convection processes might not be represented sufficiently. In summary, a good quality of CTIPe results has been demonstrated, even during extreme conditions. However, there is still room for improvement. The integration of better plasma transport and PPEF are recommended to be addressed next.

The storm driving mechanisms have been studied by analyzing the best approximate model results. Strong Joule heating in the Auroral region, driving storm wind cells during day, is visible in the model results. The storm wind cells contain equatorward meridional winds in the mid-latitude ionosphere F-region. These winds transport oxygen rich air to lower latitudes (reducing the recombination rate) and besides, they transport plasma up along the magnetic field lines, resulting in a conservation of plasma at greater altitudes. Both effects cause an increase of TEC in mid-latitudes during the day. The meridional winds are accompanied by atmospheric gravity waves, which have been noticed in TEC. In high-latitudes, intense equatorward winds are observed during the night. These are ion-driven

winds, resulting from $E \times B$-drifts across the polar cap (characterized by TOI). This effect is accompanied by frictional heating of the thermosphere. The heating of the thermosphere and the storm wind cells cause the expansion of the neutral atmosphere and composition redistribution. This result in a decrease of the $[O/N_2]$-ratio starting with the development of meridional winds. The $[O/N_2]$-ratio drop causes a TEC descent because of higher recombination. This is a typical effect of the ionosphere storm recovery. However, at high latitudes in the Auroral region, this effect is superimposed by the TOI effect.

In conclusion, CTIPe has a very good capability to reproduce thermosphere-ionosphere perturbations during storms. However, correct estimation of the forcing is a necessary requirement for achieving best model results. This case study demonstrates, a considerable impact of input data gaps in operational model results.

Acknowledgements

This work has been finalized in the frame of the INSIGTH-II project funded by the Deutsche Forschungsgemeinschaft (DFG) under the project Grant No. 273590813. The authors would like to thank the international GNSS service (IGS) for providing GNSS data under http://www.igs.org/. We also would like to thank the DEOS thermosphere web service for providing neutral density data from the CHAMP satellite and OMNIWeb from NASA for the magnetospheric input data. Also, we thank the ACE SWEPAM and ACE MAG instrument teams and the ACE Science Center for supplying the ACE data.

References

Bailey, G., 1983. The effect of a meridional E× B drift on the thermal plasma at L = 1.4. Planet. Space Sci. 31, 389–409.

Baishev, D., Borisov, G., Velichko, V., Samsonov, S., Yumoto, K., 2008. Variations in the geomagnetic field and auroras during the main phase of a large magnetic storm of November 20, 2003. Geomagn. Aeronomy 48, 201–208.

Balan, N., Alleyne, H., Otsuka, Y., Lekshmi, D.V., Fejer, B.G., McCrea, I., 2009. Relative effects of electric field and neutral wind on positive ionospheric storms. Earth Planets Space 61, 439–445.

Blanc, M., Richmond, A., 1980. The ionospheric disturbance dynamo. J. Geophys. Res. Space Phys. 85, 1669–1686.

Blanch, E., Altadill, D., Hernández-Pajares, M., et al., 2005. November 2003 event: effects on the Earth's ionosphere observed from ground-based ionosonde and GPS data. In: Annales Geophysicae, pp. 3027–3034.

Borries, C., Jakowski, N., Kauristie, K., Amm, O., Mielich, J., Kouba, D., 2017. On the dynamics of large-scale traveling ionospheric disturbances over Europe on 20 November 2003. J. Geophys. Res. Space Phys. 122, 1199–1211.

Bortnik, J., Thorne, R., O'Brien, T., Green, J., Strangeway, R., Shprits, Y., Baker, D., 2006. Observation of two distinct, rapid loss mechanisms during the 20 november 2003 radiation belt dropout event. J. Geophys. Res. Space Phys. 111, A12216.

Bruinsma, S., Tamagnan, D., Biancale, R., 2004. Atmospheric densities derived from CHAMP/STAR accelerometer observations. Planet. Space Sci. 52, 297–312.

Buonsanto, M.J., 1999. Ionospheric storms: a review. Space Sci. Rev. 88, 563–601.

Codrescu, M., Fuller-Rowell, T., Foster, J., 1995. On the importance of E-field variability for Joule heating in the high-latitude thermosphere. Geophys. Res. Lett. 22, 2393–2396.

Codrescu, M., Fuller-Rowell, T., Munteanu, V., Minter, C., Millward, G., 2008. Validation of the coupled thermosphere ionosphere plasmasphere electrodynamics model: CTIPe-Mass Spectrometer Incoherent Scatter temperature comparison. Space Weather 6, S09005.

Codrescu, M., Roble, R., Forbes, J., 1992. Interactive ionosphere modeling: a comparison between TIGCM and ionosonde data. J. Geophys. Res. Space Phys. 97, 8591–8600.

Crowley, G., Hackert, C., Meier, R., Strickland, D., Paxton, L., Pi, X., Mannucci, A., Christensen, A., Morrison, D., Bust, G., et al., 2006. Global thermosphere-ionosphere response to onset of 20 November 2003 magnetic storm. J. Geophys. Res. Space Phys. 111, A10S18.

De Franceschi, G., Alfonsi, L., Romano, V., Aquino, M., Dodson, A., Mitchell, C.N., Spencer, P., Wernik, A.W., 2008. Dynamics of high-latitude patches and associated small-scale irregularities during the October and November 2003 storms. J. Atmos. Sol. Terr. Phys. 70, 879–888.

Doornbos, E., Van Den Ijssel, J., Lühr, H., Förster, M., Koppenwallner, G., 2010. Neutral density and crosswind determination from arbitrarily oriented multiaxis accelerometers on satellites. J. Spacecraft Rockets 47, 580–589.

Ebihara, Y., Fok, M.C., Sazykin, S., Thomsen, M., Hairston, M., Evans, D., Rich, F., Ejiri, M., 2005. Ring current and the magnetosphere-ionosphere coupling during the superstorm of 20 November 2003. J. Geophys. Res. Space Phys. 110, A09S22.

Fedrizzi, M., Fuller-Rowell, T.J., Codrescu, M.V., 2012. Global Joule heating index derived from thermospheric density physics-based modeling and observations. Space Weather 10, S03001.

Foster, J., Coster, A., Erickson, P., Holt, J., Lind, F., Rideout, W., McCready, M., Van Eyken, A., Barnes, R., Greenwald, R., et al., 2005. Multiradar observations of the polar tongue of ionization. J. Geophys. Res. Space Phys. 110, A09S31.

Foster, J., Holt, J.M., Musgrove, R., Evans, D., 1986. Ionospheric convection associated with discrete levels of particle precipitation. Geophys. Res. Lett. 13, 656–659.

Fuller-Rowell, T., Codrescu, M., Moffett, R., Quegan, S., 1994. Response of the thermosphere and ionosphere to geomagnetic storms. J. Geophys. Res. Space Phys. 99, 3893–3914.

Fuller-Rowell, T., Emmert, J., Fedrizzi, M., Wiemer, D., Codrescu, M.V., Pilinski, M., Sutton, E., Viereck, R., Reader, J., Doornbos, E., 2018. How might the thermosphere and ionosphere react to an extreme space weather event? Extreme Events Geospace, 513–539.

Fuller-Rowell, T., Evans, D., 1987. Height-integrated Pedersen and Hall conductivity patterns inferred from the TIROS-NOAA satellite data. J. Geophys. Res. Space Phys. 92, 7606–7618.

Fuller-Rowell, T., Rees, D., Quegan, S., Moffett, R., Codrescu, M., Millward, G., 1996. A coupled thermosphere-ionosphere model (CTIM). STEP Report, 239.

Jakowski, N., Béniguel, Y., De Franceschi, G., Pajares, M.H., Jacobsen, K.S., Stanislawska, I., Tomasik, L., Warnant, R., Wautelet, G., 2012. Monitoring, tracking and forecasting ionospheric perturbations using GNSS techniques. J. Space Weather Space Climate 2, A22.

Kil, H., Kwak, Y.S., Paxton, L., Meier, R., Zhang, Y., 2011. O and N_2 disturbances in the F region during the 20 November 2003 storm seen from TIMED/GUVI. J. Geophys. Res. Space Phys. 116, A02314.

Mannucci, A., Tsurutani, B., Abdu, M., Gonzalez, W., Komjathy, A., Echer, E., Iijima, B., Crowley, G., Anderson, D., 2008. Superposed epoch analysis of the dayside ionospheric response to four intense geomagnetic storms. J. Geophys. Res. Space Phys. 113, A00A02.

Mansilla, G., 2004. Mid-latitude ionospheric effects of a great geomagnetic storm. J. Atmos. Sol. Terr. Phys. 66, 1085–1091.

Marsh, D., Solomon, S., Reynolds, A., 2004. Empirical model of nitric oxide in the lower thermosphere. J. Geophys. Res. Space Phys. 109, A07301.

Meier, R., Crowley, G., Strickland, D., Christensen, A., Paxton, L., Morrison, D., Hackert, C., 2005. First look at the 20 November 2003 superstorm with TIMED/GUVI: comparisons with a thermospheric global circulation model. J. Geophys. Res. Space Phys. 110, A09S41.

Millward, G., Moffett, R., Quegan, S., Fuller-Rowell, T., 1996. A coupled thermosphere-ionosphere-plasmasphere model (CTIP). STEP Handbook on Ionospheric Models, 239–279.

Millward, G., Müller-Wodarg, I., Aylward, A., Fuller-Rowell, T., Richmond, A., Moffett, R., 2001. An investigation into the influence of tidal forcing on F region equatorial vertical ion drift using a global ionosphere-thermosphere model with coupled electrodynamics. J. Geophys. Res. A. Space Phys. 106 (A11), 24733–24744.

Negrea, C., Codrescu, M., Fuller-Rowell, T., 2012. On the validation effort of the Coupled Thermosphere Ionosphere Plasmasphere Electrodynamics model. Space Weather 10 (8), 1–9.

Prölss, G., von Zahn, U., 1977. On the global morphology of negative ionospheric storms. In: Space Research XVII, pp. 433–438.

Prolss, G.W., Bird, M.K., 2004. Physics of the Earth's Space Environment: An Introduction. Springer, New York City.

Qian, L., Solomon, S.C., Kane, T.J., 2009. Seasonal variation of thermospheric density and composition. J. Geophys. Res. Space Phys. 114, A01312.

Quegan, S., Bailey, G., Moffett, R., Heelis, R., Fuller-Rowell, T., Rees, D., Spiro, R., 1982. A theoretical study of the distribution of ionization in the high-latitude ionosphere and the plasmasphere: first results on the mid-latitude trough and the light-ion trough. J. Atmos. Terr. Phys. 44, 619–640.

Richmond, A., Ridley, E., Roble, R., 1992. A thermosphere/ionosphere general circulation model with coupled electrodynamics. Geophys. Res. Lett. 19, 601–604.

Rodger, A., Wells, G., Moffett, R., Bailey, G., 2001. The variability of Joule heating, and its effects on the ionosphere and thermosphere. In: Annales Geophysicae, pp. 773–781.

Shim, J., Tsagouri, I., Goncharenko, L., Rastaetter, L., Kuznetsova, M., Bilitza, D., Codrescu, M., Coster, A., Solomon, S., Fedrizzi, M., et al., 2018. Validation of ionospheric specifications during geomagnetic storms: TEC and foF2 during the 2013 March Storm Event. Space Weather 16, 1686–1701.

Shim, J.S., Kuznetsova, M., Rasttter, L., Bilitza, D., Butala, M., Codrescu, M., Emery, B.A., Foster, B., Fuller-Rowell, T.J., Huba, J., Mannucci, A.J., Pi, X., Ridley, A., Scherliess, L., Schunk, R.W., Sojka, J.J., Stephens, P., Thompson, D.C., Weimer, D., Zhu, L., Sutton, E., 2012. CEDAR electrodynamics thermosphere ionosphere (ETI) challenge for systematic assessment of ionosphere/thermosphere models: electron density, neutral density, NmF2, and hmF2 using space based observations. Space Weather 10, S10004. https://doi.org/10.1029/2012SW000851.s10004.

Shimeis, A., Borries, C., Amory-Mazaudier, C., Fleury, R., Mahrous, A. M., Hassan, A., Nawar, S., 2015. TEC variations along an East Euro-African chain during 5th April 2010 geomagnetic storm. Adv. Space Res. 55, 2239–2247.

Weimer, D., 2005. Improved ionospheric electrodynamic models and application to calculating Joule heating rates. J. Geophys. Res. Space Phys. 110, A05306.